

Electronic structures and low-dimensional magnetic properties of the ordered rocksalt oxides $\text{Na}_3\text{Cu}_2\text{SbO}_6$ and $\text{Na}_2\text{Cu}_2\text{TeO}_6$

Shahab Derakhshan,^{1,2,*} Heather L. Cuthbert,^{1,2} and John E. Greedan^{1,2}¹Chemistry Department, McMaster University, 1280 Main Street West, Hamilton, Ontario, Canada L8S 4M1²Brockhouse Institute for Materials Research at McMaster University, 1280 Main Street West, Hamilton, Ontario, Canada L8S 4M1Badiur Rahaman³ and Tanusri Saha-Dasgupta³³S.N. Bose National Centre for Basic Sciences, JD Block, Sector III, Salt Lake City, Kolkata 700098, India

(Received 8 March 2007; published 5 September 2007)

The ordered rocksalt-type oxide $\text{Na}_3\text{Cu}_2\text{SbO}_6$ was synthesized and its magnetic properties were investigated. The broad peak in the temperature-dependent magnetic susceptibility data near 92 K is indicative of the dominant low-dimensional short-range antiferromagnetic (AF) behavior. The data are very well fitted with the AF-AF alternating linear chain model with $J_1/k = -79$ K and $J_2/J_1 = 0.39$. The high-temperature data ($T > 300$ K) exhibit Curie-Weiss behavior with a Weiss temperature of $-55(2)$ K. These results are very similar to those reported for the isostructural oxide $\text{Na}_2\text{Cu}_2\text{TeO}_6$ [J. Xu *et al.*, *Inorg. Chem.* **44**, 5042 (2005)]. Recently, it was shown [Y. Miura *et al.*, *J. Phys. Soc. Jpn.* **75**, 847071 (2006)] that an AF-ferromagnetic (F) linear chain model gives an equally good fit to the low-temperature data for both compounds and that further analysis of magnetic heat capacity data supports the AF-F model. We reinvestigate this proposal by computing the intersite hopping integrals using both the tight-binding spin dimer analysis and the N^{th} -order muffin-tin-orbital downfolding procedure for both compounds. The calculations support the AF-AF model for the antimonide. Further, the Weiss temperatures derived from the high-temperature experimental data, $T > 300$ K, are also consistent with the J values derived from the AF-AF model but not with those obtained from the AF-F alternative.

DOI: [10.1103/PhysRevB.76.104403](https://doi.org/10.1103/PhysRevB.76.104403)

PACS number(s): 75.40.-s

I. INTRODUCTION

Magnetic oxides with an ordered rocksalt structure often show low-dimensional behavior due to either the topology of the cation ordering or to orbital ordering, especially with Jahn-Teller active ions. For example, the thermodynamically stable form of LiMnO_2 with $Pm\bar{m}n$ symmetry has zigzag layers of Mn^{3+} ions and shows short-range, two-dimensional magnetic correlations over a wide temperature range before long-range order sets in below 271 K.¹ More remarkably, the metastable form of this same material, $t\text{-Li}_2\text{Mn}_2\text{O}_4$, with $I4_1/amd$ symmetry and a three-dimensional (3D) topology for the Mn^{3+} ions, shows only two-dimensional spin correlations down to 2 K.² The material $\text{Li}_4\text{MgReO}_6$, in which the Re^{6+} ($S=1/2$) ions are arrayed on a geometrically frustrated lattice, shows spin-glass behavior below 12 K and not long-range order.³

Quite recently oxides with a layered rocksalt structure, $\text{Na}_2\text{Cu}_2\text{TeO}_6$ and $\text{Na}_3\text{Cu}_2\text{SbO}_6$, have been investigated,^{4,5} which occur in distorted honeycomb crystal structures. Such a lattice structure with low coordination of magnetic ions is expected to exhibit strong magnetic fluctuations, characteristic of low-dimensional spin systems. These compounds fall in the category of quaternary cuprate-tellurate and cuprate-antimonate which have so far remained largely unexplored. The relationship between the two structures has been described before,^{4,5} so it will be reviewed briefly here. Figures 1(a) and 1(b) show the $\text{Na}_3\text{Cu}_2\text{SbO}_6$ structure viewed along the a and c axes of the $C2/m$ cell. Note the presence of layers of edge-sharing Cu-O and Sb-O octahedra separated by Na^+ ions. One Na^+ site is vacant in the tellurate phase, so

it can be considered as a defect rocksalt material. The magnetic Cu^{2+} ions lie in planes of composition $\text{Cu}_2\text{TeO}_6^{2-}$ or $\text{Cu}_2\text{SbO}_6^{3-}$ and, due to site ordering with the Te^{6+} and Sb^{5+} ions, present a slightly distorted honeycomb lattice topology, as shown in Fig. 2. There are five possible exchange pathways within the ab plane. Two possible pathways J_4 and J_5

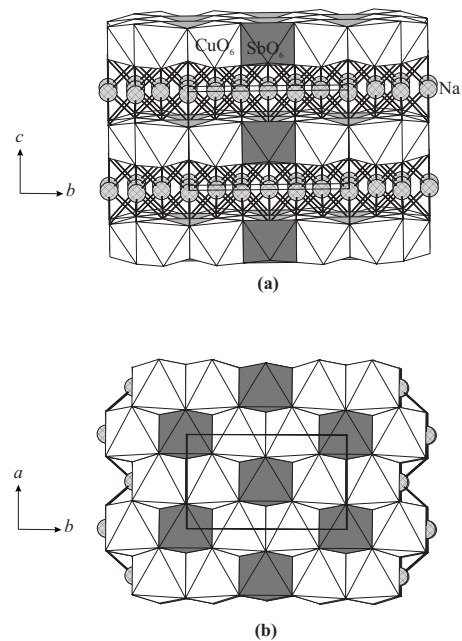


FIG. 1. Edge-sharing octahedra in $\text{Na}_3\text{Cu}_2\text{SbO}_6$ viewed along the a direction (a) and the c direction (b).

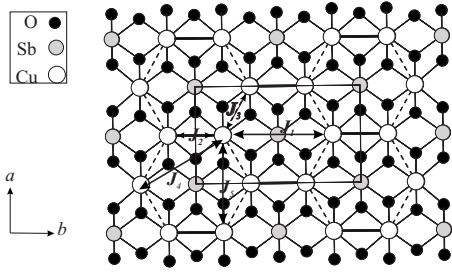


FIG. 2. Schematic representation of different possible Cu-Cu interaction pathways in the ab plane. The thick solid lines denote the shortest Cu-Cu interactions, the thin solid lines show Cu-O and Sb-O connectivity, and the dashed lines represent the shortest inter-chain Cu-Cu interactions.

are relatively long, involving fully occupied d_z^2 orbitals and, as such, their contribution is negligible. As a result, they have not been taken into account in any subsequent analysis. The three most significant nearest-neighbor exchange pathways are J_1 , J_2 , and J_3 . Depending on their signs and relative magnitudes, the magnetic dimensionality can be 0, 1, or 2 as indicated in Table I. The magnetic susceptibility data suggest a dominant dimeric or zero-dimensional interaction. Closer inspection indicates that an alternating linear chain model provides a somewhat better fit than the dimer model.^{4,5} There exists some controversy regarding the sign of the second-neighbor interaction J_2 . While one group has fit the data for $\text{Na}_2\text{Cu}_2\text{TeO}_6$ using the antiferromagnetic-antiferromagnetic (AF-AF) alternating chain model with $J_2/J_1 \sim 0.1$,⁴ Miura *et al.*⁵ have pointed out that distinguishing between the AF-AF and AF-ferromagnetic (AF-F) models is very difficult based only on the criterion of the fit quality. The AF-F model does indeed provide an excellent fit with rather different parameters—for example, $J_1/J_2 \sim -0.8$ —for both Sb- and Te-based materials. Fits to low-temperature heat capacity data appear to support the AF-F model.⁵

In an attempt to resolve this controversy, we have carried out several studies. First, the magnetic properties of $\text{Na}_3\text{Cu}_2\text{SbO}_6$ have been reinvestigated including data up to 600 K. Second, calculations using the tight-binding and more accurate N^{th} -order muffin-tin-orbital (NMTO) down-folding method⁶ have been done on both the Te and Sb compounds to determine the relative magnitudes of the relevant exchange constants by providing estimates of the corresponding hopping interactions. Finally, the observed Weiss temperatures derived from Curie-Weiss fits to high-temperature data have been compared to the values predicted from the J 's obtained from fits to the low-temperature data.

TABLE I. The different possible dimensionalities of the Cu^{2+} spin correlations.

Relative interaction magnitudes	Magnetic model
$J_2 \approx J_3 \gg J_1$	2D honeycomb
$J_1 = J_2 \gg J_3$	1D chain
$J_1 > J_2 \gg J_3$	1D alternating chain
$J_1 \gg J_2 \approx J_3$	0D dimer

TABLE II. Some selected interatomic Cu-O distances of $\text{Na}_2\text{Cu}_2\text{TeO}_6$ and $\text{Na}_3\text{Cu}_2\text{SbO}_6$ (Refs. 4 and 7).

	$\text{Na}_2\text{Cu}_2\text{TeO}_6$	$\text{Na}_3\text{Cu}_2\text{SbO}_6$
$2 \times \text{Cu-O}(1)$ (Å)	1.978	2.000
$2 \times \text{Cu-O}(2)$ (Å)	1.999	2.021
$2 \times \text{Cu-O}(1)$ (Å)	2.533	2.494

II. EXPERIMENT

A. Synthesis

The $\text{Na}_3\text{Cu}_2\text{SbO}_6$ sample was prepared according to the procedure introduced by Smirnova.⁷ For this purpose a stoichiometric mixture of Na_2CO_3 (BDH, 99%), Sb_2O_3 (Aldrich, 99.99%), and CuO (Cerac, 99.999%) powder was thoroughly ground and pressed into a pellet. The pellet was placed in an alumina boat and heated to 900 °C, was cooled down to 600 °C in 100 h in air, and finally, the furnace was turned off.

B. Phase analyses

The formation and phase purity of the olive green product were confirmed using powder x-ray diffraction employing a Guinier-Hägg camera with $\text{Cu } K\alpha_1$ radiation and a Si internal standard. A KEJ line scanner was utilized to convert the film record to digital data.

C. Magnetic measurements

Temperature-dependent magnetic susceptibility data for $\text{Na}_3\text{Cu}_2\text{SbO}_6$ were collected employing a Quantum Design MPMS superconducting quantum interference device (SQUID) magnetometer. Both zero-field cooled (ZFC) and field cooled (FC) data were obtained over the temperature range of 2–300 K at an applied field of 1000 Oe. High-temperature (310–600 K) susceptibility data were collected using an oven insert at 1000 Oe.

III. RESULTS AND DISCUSSION

A. Structural comparisons

Before turning to the magnetic properties, a brief but detailed comparison of the salient structural details of both $\text{Na}_3\text{Cu}_2\text{SbO}_6$ and $\text{Na}_2\text{Cu}_2\text{TeO}_6$ is presented in Tables II and III. As the Sb^{5+} (0.74 Å) (Ref. 8) ion is slightly larger than Te^{6+} (0.70 Å) (Ref. 8), there is an overall increase in cell volume, the b axis length, and the interatomic distances within the ab plane. The distances and angles relevant to the three identified exchange pathways J_1 , J_2 , and J_3 are indicated in Table III.

B. Magnetic susceptibilities

The high-temperature magnetic susceptibility data of $\text{Na}_3\text{Cu}_2\text{SbO}_6$ from 310 to 600 K (Fig. 3) were seen to fit very well to the Curie-Weiss law, $\chi = \frac{C}{T-\theta}$. The fitting parameters are $C=1.019(4)$ emu/mol for the Curie constant and

TABLE III. Some selected structural parameters of $\text{Na}_2\text{Cu}_2\text{TeO}_6$ and $\text{Na}_3\text{Cu}_2\text{SbO}_6$ (Refs. 4 and 7.)

	$\text{Na}_2\text{Cu}_2\text{TeO}_6$	$\text{Na}_3\text{Cu}_2\text{SbO}_6$
b (Å)	8.675	8.867
V (Å ³)	269.05	269.81
(Cu-Cu)[J_1] (Å)	5.82	5.91
(\angle Cu-O-O)[J_1] (deg)	139	137.2
(Cu-Cu)[J_2] (Å)	2.86	2.96
(\angle Cu-O-Cu)[J_2] (deg)	91.3	95.3
(Cu-Cu)[J_3] (Å)	3.21	3.20
(\angle Cu-O-Cu)[J_3] (deg)	90.0	89.6

$\theta = -55(2)$ K for the Weiss constant. This Curie constant corresponds to an effective magnetic moment μ_{eff} of $2.02(1)\mu_B$ per Cu^{2+} ($3d^9$, $S = \frac{1}{2}$), which is higher than spin only value of $1.73\mu_B$ which is typical for Cu^{2+} . The negative value for the Weiss constant is indicative of predominant AF interactions.

Concerning the low-temperature data (2–300 K), since there was no significant difference between the ZFC and FC data sets, only the ZFC data will be considered for the purposes of discussion. The sharp increase in susceptibility at low temperatures (2–19 K) (Fig. 4) can be attributed to a paramagnetic impurity. A broad maximum in the susceptibility is present, near 92 K, which is indicative of the low-dimensional, short-range antiferromagnetic nature of the magnetism of this compound.

Due to strong similarities with the data for the tellurate, the AF-AF alternating chain model was applied in this case as well. A Curie-Weiss term was added to model the sharp upturn at low temperatures. This should not be confused with the Curie-Weiss fit of the high-temperature data of Fig. 3. As well, a temperature-independent term χ_{TIP} was added. The following function was employed:⁹

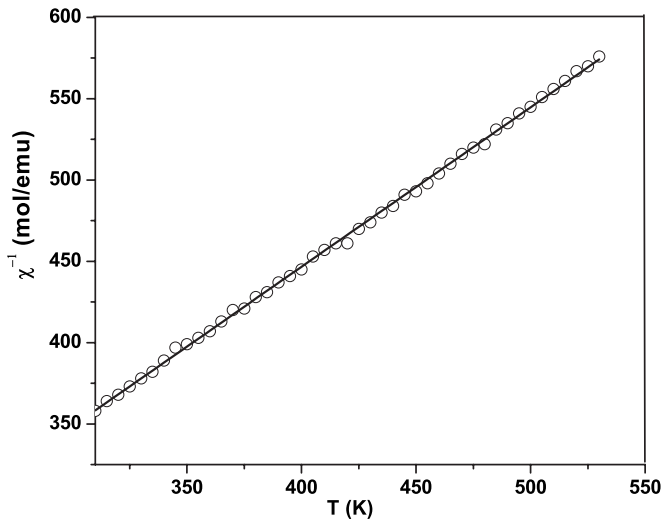


FIG. 3. Curie Weiss fit of data in the high-temperature paramagnetic region. The open circles represent the data points and the solid line is the fit.

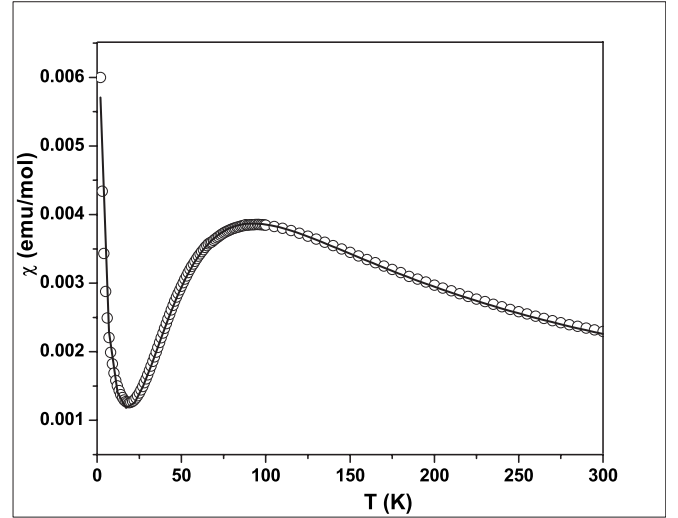


FIG. 4. Zero-field-cooled magnetic susceptibility data for $\text{Na}_3\text{Cu}_2\text{SbO}_6$. The open circles represent the ZFC data and the solid line is the fit, based on the AF-AF alternating chain model.

$$\chi_M = \frac{Ng^2\mu_B^2(A+Bx+Cx^2)}{k_B T(1+Dx+Ex^2+Fx^3)} + \frac{C_{\text{impurity}}}{T - \theta_{\text{impurity}}} + \chi_{TIP},$$

where g is the Landé g factor, $\frac{N_B}{k_B} = 0.375$, $x = \frac{|J_1|}{k_B T}$, and the constants are as follows (with $\alpha = \frac{J_2}{J_1}$ and $0 \leq \alpha \leq 0.4$):

$$A = 0.25,$$

$$B = -0.12587 + 0.22752\alpha,$$

$$C = 0.019111 - 0.13307\alpha + 0.50967\alpha^2 - 1.33167\alpha^3 + 1.0081\alpha^4,$$

$$D = 0.10772 + 1.4192\alpha,$$

$$E = -0.0028521 - 0.42346\alpha + 2.1953\alpha^2 - 0.82412\alpha^3,$$

$$F = 0.37754 - 0.067022\alpha + 6.9805\alpha^2 - 21.678\alpha^3 + 15.838\alpha^4.$$

This is a general model, which includes the 0D dimer with $\alpha=0$ and simple 1D chain with $\alpha=1$. The fitted values are summarized in Table IV, which also includes the results for the tellurate material for comparison. The values for the antimonate material are in good agreement with those obtained by Miura *et al.* for the same model.⁵

C. Computational methods

1. Tight-binding, magnetic dimer model

At this stage, computational estimates of the various J 's are needed in order to interpret these results. In previous work on the tellurate material,⁴ the extended Hückel, spin dimer analysis¹⁰ was employed. In these computations the intersite hopping energy ($\Delta\epsilon$) is estimated using the CAESAR

TABLE IV. The obtained values from AF-AF alternating chain model fit to ZFC data of $\text{Na}_2\text{Cu}_2\text{TeO}_6$ and $\text{Na}_3\text{Cu}_2\text{SbO}_6$.

	g	J_1/k_B (K)	α	C (emu K/mol)	θ (K)	χ_{TIP} (emu/mol)
$\text{Na}_2\text{Cu}_2\text{TeO}_6^{\text{a}}$	2.03(1)	-134.6(3)	0.10(1)	0.0070(4)	1.2(2)	0.00066(2)
$\text{Na}_3\text{Cu}_2\text{SbO}_6$	1.972(6)	-79.6(6)	0.39(1)	0.027(1)	-2.3(1)	0.00022

^aReference 4.

package.¹¹ Assuming that $J \sim (\Delta e)^2/U$ and that U is constant, the relative magnitude of the various J 's can be determined. Calculations on the spin dimer model for the antimonate yielded the results shown in Table V which are compared with those reported for the tellurate.⁴

Note that in both cases, J_1 , which involves the longest Cu-Cu pathway, is, nonetheless, the largest interaction by far. Second in magnitude is J_2 , of order ~ 0.1 of J_1 . J_3 is much smaller, ~ 0.01 of J_1 . Comparing the tellurate and antimonate phases the calculated $J_1(\text{Sb})/J_1(\text{Te})$ ratio is 0.54 compared to the experimental ratio of 0.59, which is an acceptable agreement. However, the observed and calculated J_1/J_2 ratios (α in Table IV and "Rel" in Table V) are in poor correspondence.

2. Local density approximation calculation

It is of considerable interest to apply a more rigorous computational method to this problem. Recently, the so-called NMTO downfolding approach has been proposed for such purposes.⁶ This involves, initially, a full self-consistent local density approximation (LDA) calculation followed by a particular post-processing analysis. Specifically, this involves an energy-selective downfolding in which a few bands of interest are obtained from the full band LDA result by integrating out degrees of freedom that are not of interest, called passive channels, and retaining the few degrees of freedom which are of interest, called active channels. The few-band, downfolded Hamiltonian is thus constructed in the basis of effective NMTOs which have the central character of an active orbital and the tails are shaped according to passive downfolded orbital characters. For a well-converged, isolated set of downfolded bands, these effective NMTOs span the same Hilbert space as the Wannier functions of the corresponding downfolded bands. The real-space representation of the downfolded Hamiltonian in the basis of the downfolded NMTO's provides the information on the effective intersite hoppings.

Self-consistent electronic structure calculations were carried out within the LDA framework of the density functional theory (DFT) in the tight-binding linear muffin-tin-orbital

TABLE V. $(\Delta e)^2$ for the various exchange pathways in both $\text{Na}_2\text{Cu}_2\text{TeO}_6$ and $\text{Na}_3\text{Cu}_2\text{SbO}_6$ calculated on the spin dimer model.

Pathway	Te $(\Delta e)^2$ (meV) ²	Rel.	Sb $(\Delta e)^2$ (meV) ²	Rel.
J_1	10200	1	5224	1
J_2	3320	0.33	295	0.06
J_3	130	0.01	16	0.003

(TB-LMTO) basis.¹² The basis set consisted of Cu *spd*, Te or Sb *sp*, O *sp*, and Na *s* orbitals. Five (Te) or four (Sb) different classes of empty spheres were used to space fill the system. The band structure and corresponding density of states are shown in Fig. 5.

The orbital characters indicated in the figure are obtained by choosing the local coordinate system with the local z axis pointing along the long Cu-O(1) bond and the local y axis pointing along the short Cu-O(1) bond. The distorted octahedral environment of the Cu^{2+} ion sets the energy of the $3d_{x^2-y^2}$ orbital as the highest. Consistent with this picture, there are two bands of $d_{x^2-y^2}$ symmetry (there are two Cu atoms per unit cell) split off from the other bands, spanning an energy range from -0.4 eV to 0.2 eV with the zero energy set at the LDA Fermi level. The energy bands dominated by other d characters, such as d_{xy} , d_{xz} , d_{yz} , and d_z^2 , are located within the energy range -2.4 and -1.2 eV, separated by a gap of ~ 0.8 eV from the $d_{x^2-y^2}$ bands. The O p -dominated bands appear at ~ -6 to -3 eV. There is only a negligible contribution from Na states to the bands crossing the Fermi level and a small but non-negligible mixing from Te (Sb) states as is more evident in the plot of effective NMTO's to be presented below.

Note that in the low-energy range, the LDA calculation leads to two almost half-filled bands—i.e., to a metallic state. It is well known that the LDA fails to describe the correct insulating ground state for strongly correlated electron systems, as is the case here. The inclusion of the missing correlation beyond the LDA provides the insulating ground state. This was checked by treating the correlation within the LDA+U framework. While the LDA fails to provide the correct ground state for these materials, it describes the chemical bonding aspects correctly and is highly successful in deriving the microscopic model.

NMTO downfolding model. The few-band, downfolded Hamiltonian was constructed from the effective Cu $d_{x^2-y^2}$ by integrating out all degrees of freedom associated with Te, Na, and O and the Cu t_{2g} and d_z states. This choice is driven by the fact that the Cu^{2+} state is described by a half-filled $d_{x^2-y^2}$ orbital. Therefore, these are the bands which appear close to the Fermi level and dominate the low-energy Hamiltonian. The downfolded band structure is shown in Fig. 6 along with the full LDA result.

With choice of two energy points of expansion, marked as $E0$ and $E1$ in the figure, the downfolded bands are indistinguishable from the full band structure within the region of interest. This indicates excellent convergence of the downfolded $d_{x^2-y^2}$ bands which in the present case form an isolated set of bands. The underlying NMTOs, therefore, are the corresponding Wannier functions which are plotted in Fig. 7.

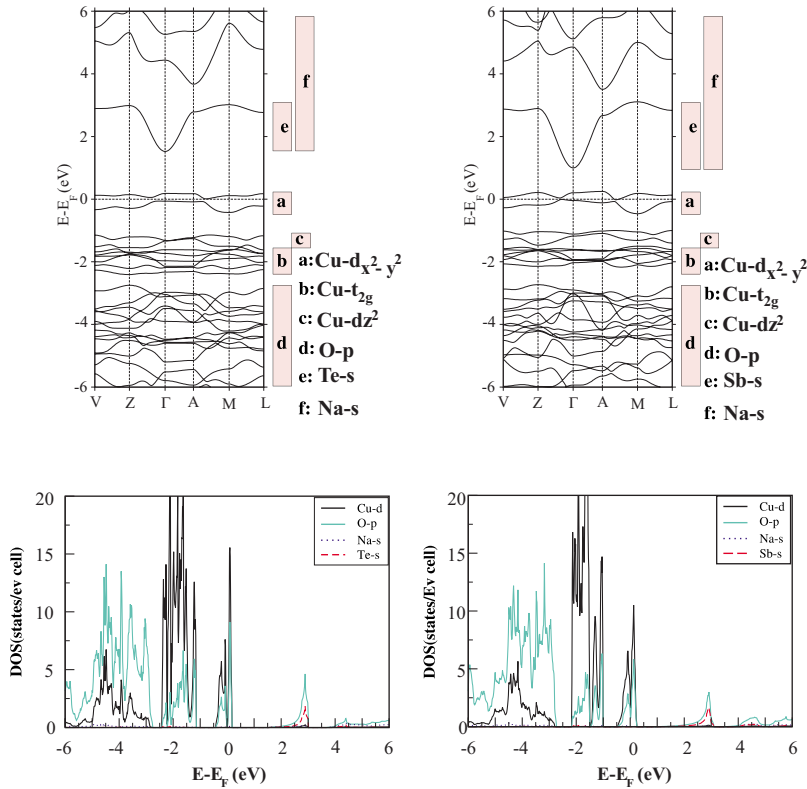


FIG. 5. (Color online) LDA band structure (top panel) and orbital-projected density of states (bottom panel) of tellurate (left) and antimonate (right). The bands are plotted along the high-symmetry points of the monoclinic BZ. The zero-point energy is set at the LDA Fermi energy (E_F) in both panels. The energy regions with the respective dominant orbital characters are marked in the top panel.

The central part has $3d_{x^2-y^2}$ symmetry with the choice of local coordinate system as stated above, while the tails are shaped according to O p symmetry to take into account hybridization effects. Shown are the orbital shapes with two different lobes colored differently. We note the $pd\sigma$ antibonds formed between Cu $d_{x^2-y^2}$ and O p . A careful look at the O p -like tails reveals that one of the lobes is enlarged with respect to the other and bends towards the Te/Sb site which in turn points towards the non-negligible contribution of Te/Sb, in providing the mediating pathway. This feature is more pronounced for $\text{Na}_2\text{Cu}_2\text{TeO}_6$ than for $\text{Na}_3\text{Cu}_2\text{SbO}_6$, giving rise to a higher value of J_1 in the case of the Te compound compared to that of the Sb compound as discussed in the following.

The real-space representation of the downfolded Hamiltonian, $H_{TB} = \sum_{ij} t_{ij} (\hat{c}_i^\dagger \hat{c}_j + \text{h.c.})$, provides the information of

the effective hopping interaction t_{ij} , between the Cu^{2+} ions at sites i and j . Such estimates of the effective hopping integrals are useful in defining the underlying low-energy magnetic model, in the sense that the effective Cu-Cu hopping integral t can be related to the Cu-Cu magnetic exchange coupling interaction J via a second-order perturbative treatment within the framework of a many-body Hubbard-like model. Assuming that these couplings are AF and neglecting the F contributions, J_{AFM} can be estimated as $\sim 4t^2/U$ where U is the effective on-site Coulomb repulsion on the Cu site.

Though such an approach may be quite legitimate for the exchange interaction J_1 with the Cu-O-O angle close to 140° , for interactions like J_2 and J_3 where Cu-O-Cu angles are reduced considerably from 180° , one needs to be more care-

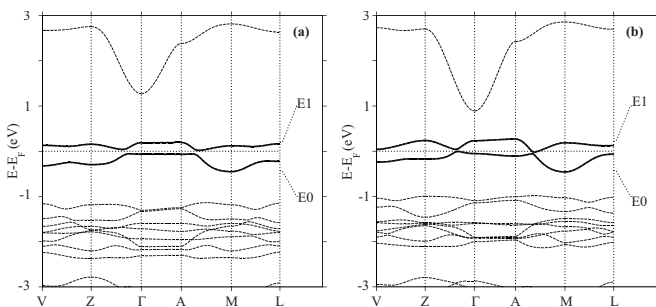


FIG. 6. Bands obtained with massively downfolded Cu $d_{x^2-y^2}$ basis (in thick lines) compared to full LDA band structure (in thin dashed lines) for tellurate (a) and antimonate (b). The NMTO energy points E_n spanning the region of interest are shown on the right-hand side.

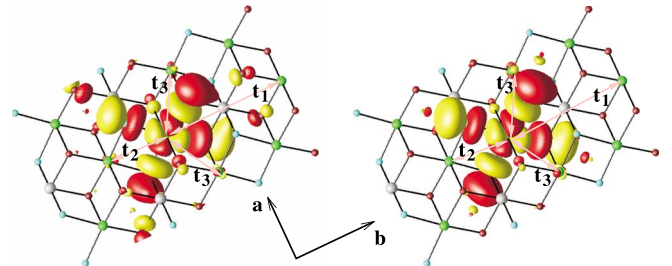


FIG. 7. (Color online) The effective orbitals corresponding to the downfolded Cu $d_{x^2-y^2}$ calculations viewed for tellurate (left) and antimonate (right). Plotted are orbital shapes (constant-amplitude surfaces) with lobes of opposite signs colored as red (dark gray) and gold (light gray). The $d_{x^2-y^2}$ orbital is defined with the choice of the local coordinate system with the y axis pointing along the short Cu-O(1) bond and the x axis pointing along the Cu-O(2) bond within the square plane.

TABLE VI. Intersite hopping energies calculated from the NMTO downfolding model for $\text{Na}_2\text{Cu}_2\text{TeO}_6$ and $\text{Na}_3\text{Cu}_2\text{SbO}_6$.

Pathway	Te t (meV)	Te t^2 (meV) ²	Rel.	Sb t (meV)	Sb t^2 (meV) ²	Rel.
J_1	139	19321	1	124	15376	1
J_2	14	196	0.01	45	2025	0.13
J_3	38	1444	0.07	31	961	0.06

ful. For this purpose, we have carried out total energy calculations with different spin arrangements at various Cu sites. Comparison of the total energies with AF spin alignment between Cu sites connected via J_2 pathways to those for F spin alignment shows the former to be lower in energy, thus proving J_2 to be AF, unequivocally.

In Table VI, we present the values of the effective hopping integrals, t_j , for the relevant magnetic exchange pathways. We also include t_j^2 by which the relative strengths of the various magnetic interactions can be obtained as $J \sim t^2/U$. These results can be compared directly with those of Table V obtained from the TB spin dimer analysis.

Both the TB and NMTO downfolding methods find that J_1 is overwhelmingly the strongest exchange pathway for both materials. The predicted $J_1(\text{Sb})/J_1(\text{Te}) \sim 0.8$ is a bit larger than the observed ratio of ~ 0.6 and, oddly, the TB spin dimer result is closer to experiment. For the Te phase, both J_2 and J_3 are of the order 10^{-2} of J_1 , suggesting that this material is close to a pure Bleaney-Bowers dimer. This is roughly consistent with experiment, as $\alpha \sim 0.1$ (Table IV).

The calculations predict a stronger J_2 interaction for the Sb phase, $J_2(\text{Sb})/J_1(\text{Sb}) \sim 0.13$, whereas the experimental result is ~ 0.4 . Nonetheless, this is an improvement over the TB calculation for which α is found to be ~ 0.06 . As well, NMTO predicts that $J_2(\text{Sb})/J_1(\text{Sb}) > J_2(\text{Te})/J_1(\text{Te})$ which is observed experimentally, while the TB method predicts the opposite. Perhaps surprisingly, $J_3(\text{Te}) > J_2(\text{Te})$, but both are very small relative to J_1 . One also needs to remember that these estimates are obtained via a t^2/U kind of relation, which is not strictly valid for the J_2 and J_3 pathways.

As mentioned, Miura *et al.*⁵ has studied the magnetic behaviors of both $\text{Na}_2\text{Cu}_2\text{TeO}_6$ and $\text{Na}_3\text{Cu}_2\text{SbO}_6$. They have pointed out, correctly, that it is very difficult to distinguish between the AF-AF and AF-F alternating chain models based solely on the fitting of the low-temperature susceptibility data. Furthermore, it was argued that an analysis of the magnetic component of the specific heat data can be used to discriminate between the two models and these data were interpreted in favor of the AF-F model with J_1 and J_2 of comparable magnitudes, $\alpha \sim -0.8$. This approach is not without difficulty. In particular, the isolation of the magnetic contribution from the total specific heat can be problematic, as a good lattice match material is needed, given that the magnetic contribution to the specific heat extends to rather high temperatures. For this purpose $\text{Na}_3\text{Zn}_2\text{SbO}_6$ was chosen, which is isostructural with $\text{Na}_3\text{Cu}_2\text{SbO}_6$, but of course there is no static Jahn-Teller distortion at the Zn^{2+} site which will influence the phonon spectrum and introduce some uncertainty into the subtraction procedure.

Apart from these potential experimental difficulties, it should be noted that neither computational method predicts a

J_2 which is of comparable magnitude to J_1 with either sign for both materials. As well, there exists a rather simple experimental test which can distinguish between the AF-AF and AF-F linear chain models for these materials. By analysis of the high-temperature susceptibility, the models can be compared to the mean-field result for the Weiss temperature θ_c . In the high-temperature regime $T > 300$ K, the Curie-Weiss law is seen to describe the data very well. The relationship between the Weiss temperature and the various exchange constants J_m is well known and given by¹³

$$\theta = \frac{2S(S+1)}{3k_B} \sum_{m=1}^N z_m J_m, \quad (1)$$

where θ is the Weiss constant, z_m is the number of m th nearest neighbors of a given atom, J_m is the exchange interaction between m th neighbors, and N is the number of sets of neighbors for which $J_m \neq 0$. For both systems with $S = \frac{1}{2}$ and $z_1 = z_2 = 1$; i.e., neglecting the J_3 contribution the relationship is simplified to

$$\theta = \frac{J_1 + J_2}{2k_B}. \quad (2)$$

In Table VII the observed θ values are compared with those derived from Eq. (2) and the J 's obtained from the fits to the low-temperature data with both the AF-AF and AF-F linear chain models.

Clearly, the AF-AF linear chain model is in much better agreement with the observed Weiss temperatures for both materials. In fact, the value derived from the AF-F model for the antimonate is actually of the opposite sign to that observed.

TABLE VII. Comparison of observed and calculated Curie-Weiss θ temperatures for both the AF-AF and AF-F linear chain models for $\text{Na}_2\text{Cu}_2\text{TeO}_6$ and $\text{Na}_3\text{Cu}_2\text{SbO}_6$.

	$\text{Na}_2\text{Cu}_2\text{TeO}_6$	$\text{Na}_2\text{Cu}_2\text{TeO}_6$	$\text{Na}_3\text{Cu}_2\text{SbO}_6$	$\text{Na}_3\text{Cu}_2\text{SbO}_6$
	AF-AF	AF-F	AF-AF	AF-F
J_1/k (K) ^a	-135	-136	-80	-83
J_2/k (K) ^a	-14	108	-31	105
θ_{calc} (K)	-75	-14	-56	11
θ_{obs} (K)	-87(6)	-87(6)	-55(2)	-55(2)

^aNote that in Ref. 5 the exchange Hamiltonian is written as $J(S_i \cdot S_j)$ whereas, in Ref. 4 and this work $-2J(S_i \cdot S_j)$ is used. Therefore, the J values quoted in Ref. 5 will be of the opposite sign and of twice the magnitude as those in Ref. 4 and the present work. The values in this table have been converted, accordingly.

IV. SUMMARY AND CONCLUSIONS

The magnetic properties of $\text{Na}_3\text{Cu}_2\text{SbO}_6$ have been investigated and compared to those for the structurally related material $\text{Na}_2\text{Cu}_2\text{TeO}_6$. Two computational methods, the tight-binding spin dimer model and the N^{th} -order muffin-tin-orbital downfolding method, have been used to calculate the intersite hopping energies of the various exchange pathways. We also used total energy calculations of different spin configurations to define the sign. Both methods find that the dominant exchange J_1 is through a Cu-O-Te(Sb)-O-Cu linear pathway and is strongly AF. As well, J_2 is found to be AF. J_2/J_1 is $\sim 10^{-2}$ for the Te phase but ~ 0.15 for the Sb material. These results are compared with each other and with experiment, and the differences are discussed. A controversy concerning whether the AF-AF or AF-F alternating chain

model is appropriate for these materials is addressed both by computation and by experiment, specifically through measurement of the high-temperature, $T > 300$ K, susceptibility and comparison of observed and calculated Weiss temperatures. On the basis of both analyses it can be concluded that the AF-AF alternating chain is the appropriate model for both compounds.

ACKNOWLEDGMENTS

We thank Paul Dube for his assistance in collecting magnetic susceptibility data. J.E.G. acknowledges the Natural Sciences and Engineering Research Council of Canada for the financial support of this work. H.L.C. also thanks the NSERC for support. T.S.D. acknowledges Swarnajayanti for support.

*Author to whom correspondence should be addressed. derakh@mcmaster.ca

¹J. E. Greedan, N. P. Raju, and I. J. Davidson, *J. Solid State Chem.* **28**, 209 (1997).

²A. S. Wills, N. P. Raju, C. Morin, and J. E. Greedan, *Chem. Mater.* **11**, 1936 (1999).

³M. Bieringer, J. E. Greedan, and G. Luke, *Phys. Rev. B* **62**, 6521 (2000).

⁴J. Xu, A. Assoud, N. Soheinia, S. Derakhshan, H. L. Cuthbert, J. E. Greedan, M. H. Whangbo, and H. Kleinke, *Inorg. Chem.* **44**, 5042 (2005).

⁵Y. Miura, R. Hirai, Y. Kobayashi, and M. Sato, *J. Phys. Soc. Jpn.* **75**, 847071 (2006).

⁶O. K. Andersen and T. Saha-Dasgupta, *Phys. Rev. B* **62**, R16219

(2000) and references therein.

⁷O. A. Smirnova, *J. Solid State Chem.* **178**, 1165 (2005).

⁸R. D. Shannon, *Acta Crystallogr., Sect. A: Cryst. Phys., Diffr., Theor. Gen. Crystallogr.* **32**, 751 (1976).

⁹J. W. Hall, W. E. Marsh, R. R. Weller, and W. E. Hatfield, *Inorg. Chem.* **20**, 1033 (1981).

¹⁰M. H. Whangbo, H. J. Koo, and D. J. Dai, *J. Solid State Chem.* **176**, 417 (2003).

¹¹J. Ren, W. Liang, and M. H. Whangbo (unpublished).

¹²Stuttgart LMTO code, O. K. Andersen and O. Jepsen, *Phys. Rev. Lett.* **53**, 2571 (1984).

¹³J. S. Smart, *Effective Field Theory of Magnetism*, Philadelphia & London (Saunders, Philadelphia, 1966).